NANO LETTERS

LETTER

pubs.acs.org/NanoLett

Correlation between Droplet-Induced Strain Actuation and Voltage Generation in Single-Wall Carbon Nanotube Films

Zheng Liu,[*,†,‡,§] Lijun Hu,[‡,§] Ji Liu,[‡,§] Caiyu Qiu,[‡,§] Haiqing Zhou,[‡,§] Daniel P. Hashim,[†] Gang Shi,[†] Cheng Peng,[†] Sina Najmaei,[†] Lianfeng Sun,[*,†] Jun Lou,[*,†] and Pulickel M. Ajayan[*,†]

[†]Department of Mechanical Engineering & Materials Science, Rice University, Houston, Texas 77005, United States

[‡]National Center for Nanoscience and Technology, Beijing 100190, China

[§]Graduate School of Chinese Academy of Sciences, Beijing 100049, China

Supporting Information

ABSTRACT:

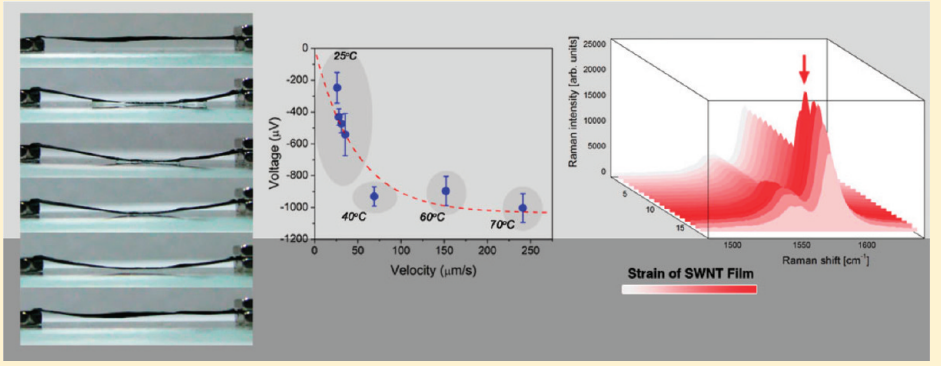

In this paper, a method of strain actuation of single-walled carbon nanotube (SWNT) films using droplets is examined, and the physical origin of an open-circuit voltage (Voc)—observed across the film during this process—is explored. We demonstrate that droplet actuation is driven by the formation of a capillary bridge between the suspended SWNT films and the substrates, which deforms the films by wetting forces during evaporation. The induced strain is further evaluated and analyzed using dynamic Raman and two-dimensional correlation spectra. Supported by theoretical calculations, our experiments reveal the time and strain dependency of the capillary bridge's midpoint directional movement. This relationship is applied to display the correlation between the induced strain and the measured Voc.

KEYWORDS: Single-wall carbon nanotube film, capillary bridge, strain, two-dimensional Raman correlation spectroscopy, open-circuit voltage, fluctuating Coulombic field

Single-walled carbon nanotubes (SWNTs) have attracted extensive interest in engineering fields due to their superb conductivity, stability, and mechanical flexibility. Traditionally, SWNTs have been used as a component of strain gauges in tensile test performances. Their outstanding tensile strength and high sensitivity,[1−4] make them an excellent candidate for strain sensors. A four-point probe method has been widely adopted to measure their resistance change during such tests.[2,5−8] However, various growth conditions and post-treatment methods have led to a significant discrepancy in the mechanical performance of SWNTs. The atomic force microscope (AFM)[9,10] is an alternative tool for the evaluation of their tensile performance. However, this method is limited to small scale samples, such as individual SWNTs and thin carbon nanotube bundles. In this paper, we report on a new approach to strain actuation in which we employ droplets to deform the free-standing SWNT films. This strain actuation is achieved through wetting forces at the interface of the droplet and the SWNT. The magnitude of the induced strain is estimated by a simplified beam theory, and strain in the range of 0.1−0.6% is controlled by adjusting the spacing between the SWNT and the substrate. Furthermore, an open-circuit voltage (Voc) was measured across the SWNT, during the deformation process. A capillary-bridge-based model suggests a correlation between the voltage and the strain within the physical scenario of the fluctuating Coulombic field. Our results demonstrate that this simple procedure provides a quick, nondestructive, replicable method to evaluate the tensile performance of SWNT films[11−13] of different sizes and thicknesses. Moreover, by correlation of the voltage and strain in SWNT films, this system can be used as a potential high-performance voltage-based strain sensor.

The SWNT films used in this work are prepared using floating catalytic chemical vapor deposition. Large-scale SWNT films are deposited on the quartz tube walls after approximately 6 h of

Received: June 6, 2011
Revised: October 18, 2011
Published: October 28, 2011

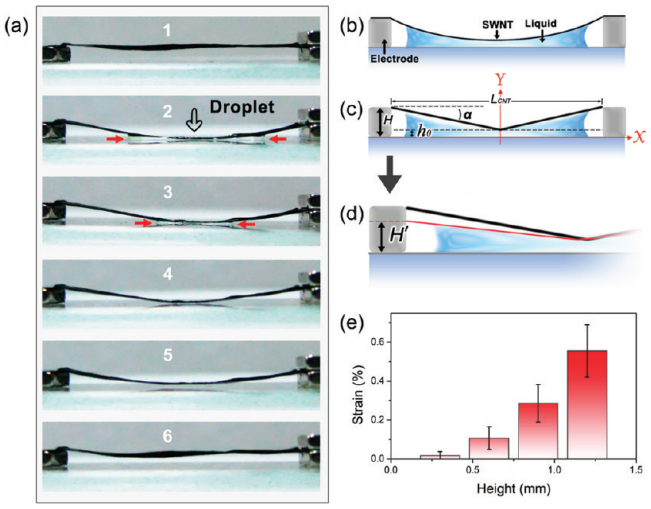

Figure 1. Deformation of a SWNT film induced by an ethanol droplet. (a) Six consecutively captured photos of the SWNT film during its deformation. (b, c) Illustration of a capillary bridge between the SWNT film and the substrate, and the corresponding simplified beam model for strain estimation. (d) Illustration of controlling the separation distance *H*. (e) Stains in SWNT films as a function of *H*.

growth. These films are cut into rectangles, placed on two electrodes, and are fixed by a copper conducting tape to ensure proper contact (see Figures S1−S3, Supporting Information).

To illustrate the mechanism of actuation, a complete deformation cycle of the SWNT films is shown in Figure 1a, frames 1−6. A drop of ethanol (~30 μL) is placed on the free-standing SWNT film (Figure 1a-1 and Figure 1a-2). This droplet drags the film down, forming a capillary bridge.[14] The slow, natural evaporation of the ethanol results in the shrinkage of the liquid to its midpoint (Figure 1a-3). Once the ethanol has almost evaporated, the film reaches a maximum strain (Figure 1a-4). Subsequent to the evaporation of the remaining ethanol on the substrate (Figure 1a-5), the film is released and restored to its free-standing state (Figure 1a-6).

Figure 1b illustrates the formation of capillary bridge after placing droplet on the SWNT film. The strain in SWNT film is estimated by a simplified beam theory (Figure 1c)

$$\varepsilon = 2\sqrt{(H(\alpha) - h_0)^2 + (L_{CNT}/2)^2}/L_{CNT} - 1 \qquad (1)$$

where ε is the maximum strain in SWNT film, H is the separation distance between the film and substrate, h_0 (0−0.3 mm) is the separation distance between the substrate and the lowest point of the SWNT after formation of a capillary bridge, L_{CNT} (20 mm) is the original length of the film, and α is the slant angle of the SWNT with respect to the substrate. To manage the magnitude of the strain on the film, the separation distance between the SWNT film and the substrate is controlled from 0.3 to 1.2 mm (Figure 1d). The consequent tensile force for these different strains is estimated using $F = EA_0\varepsilon$. Here, E is the Young's modulus with a value of roughly 5 GPa[11] for SWNT films, A_0 is the original cross-sectional area of the film (~2 mm × 1 μm), and ε is the strain on the film. The dependence of strain, ε, on the separation distance, H, is shown in Figure 1e. The largest strain produced in our experiments is about 0.6% (corresponding to a separation distance of 1.2 mm, slant angle α of ~6.0°, and a tensile force of ~56mN (see Figure S4 and Table 1, Supporting Information). The smallest strain generated was less than 0.1% (corresponding to a separation distance of 0.3 mm, a slant angle α of ~0.9°, and a tensile force of ~2mN).

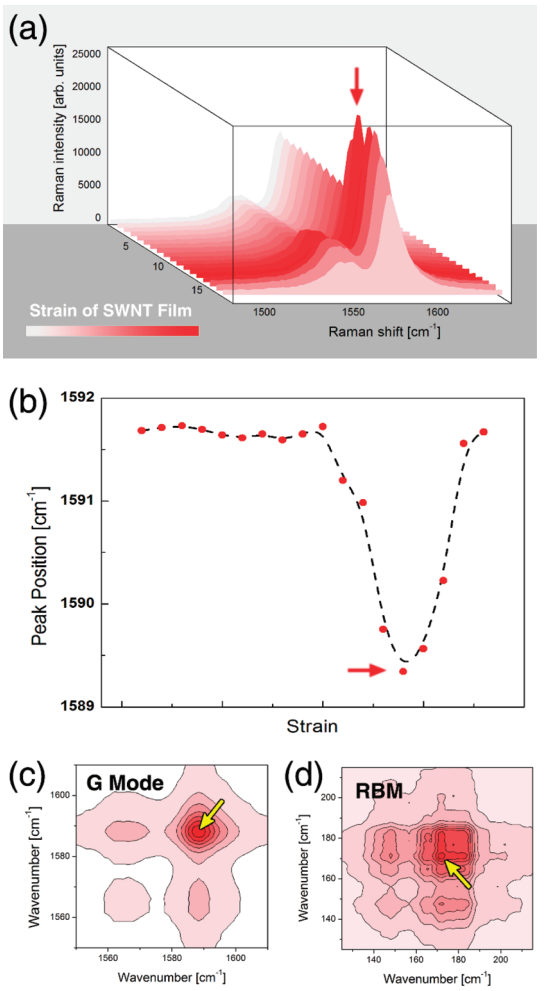

Figure 2. Raman spectroscope results for the suspended SWNT film during its deformation. (a) Raman spectra dependence on the strain of SWNT film. The color bar stands for the strain level during the deformation of film. (b) Change of G band peak positions during the deformation. The G band shows a downshift under strain. Both red arrows indicate maximum strain level, corresponding to the situation shown in Figure 1a-4. (c, d) Synchronous 2D Raman correlation spectra with wavenumber ranging from 1550 to 1610 cm^{-1} (G mode), and from 125 to 215 cm^{-1} (RBM), respectively. Yellow arrows show the most susceptible peak locations to the change of strain.

Raman spectroscopy is a powerful tool to analyze the generation and evolution of strain during the deformation of the SWNT films. This is done in a semiquantitative manner by associating the strain to the changes in the Raman band positions of carbon nanotubes.[2,15−17] The Raman spectra are collected during the deformation cycle of the film, using a Raman microscope (Renishaw inVia), with a laser wavelength of 514 nm. Figure 2a illustrates these spectra in a waterfall graph, indicating the intensity and peak position of the G mode (with upper and lower frequency components G^+ and G^-, respectively). For the first 11 spectra, there was little change in the intensity and band positions. As a result of the liquid shrinkage and its consequently induced strain on the film, a rapid increase in G peak intensity and a down-shift in the G band position can be

dx.doi.org/10.1021/nl201910j |*Nano Lett.* 2011, 11, 5117–5122

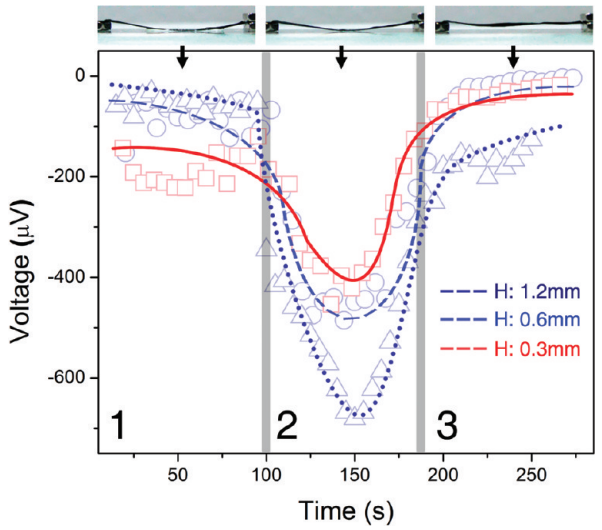

Figure 3. Generation of open-circuit voltages across SWNT films during their deformation. Voltage vs time plot shows behaviors of induced voltage with time. Corresponding typical capillary bridges are shown on top of the plot. The data shown in triangles, circles, and squares correspond to a separate distance H of 1.2, 0.6, and 0.3 mm, respectively.

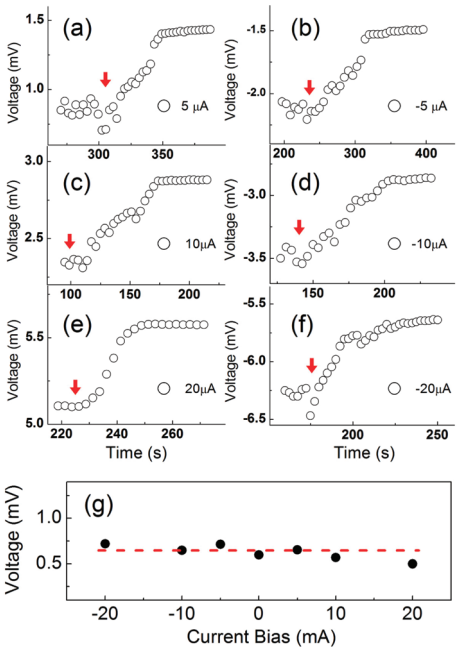

Figure 4. Induced voltage versus different current bias. (a−f) Induced voltage under current bias of 5, −5, 10, −10, 20, and −20 μA, respectively . It can be found that the voltage will decrease and then return to its original value during the deformation of the SWNT film in all six situations. (g) For different current bias, the maximum induced voltage is around 500−600 μV.

found. The downshift of the G bands originates from the elongation of the carbon−carbon bonds by strain, which weakens the bonds and therefore lowers their vibrational frequency.[18] The intensity of G band reached a maximum value at the 13th spectrum, as indicated by the red arrow in Figure 2a. Later, the intensity decreased to the original value when there was no ethanol remaining on the substrate. Figure 2b illustrates the relationship between the strain and the G^+ band position. This downshift in the band position and its relationship with strain are in agreement with previously reported studies.[18,19,20] Maximum strain attained in these experiments is represented by a downshift of ~2 cm^{-1} (denoted by an arrow).

For further analysis of the deformation process, contour maps of two-dimensional synchronous correlation spectra[21] (intensity versus time) are shown in panels c and d of Figure 2. The variations in the intensity of the correlation spectra are observed in both G and radial breathing modes (RBM). Two diagonal peaks (autopeaks), located at 1590 and 1566 cm^{-1} corresponding to the G^+ and G^- modes, respectively, are marked in panels c and d of Figure 2. The G^+ mode has significantly stronger autopeak intensity relative to the G^- mode, suggesting that the G^+ mode is more susceptible to change as strain is imposed on the SWNT films. Due to the indistinguishable collective effects of SWNTs of varying diameters, the RBM contour map in panel d is not as clear as the G mode. The variations observed in the spectral intensity range from 165 to 188 cm^{-1}. The Raman peak located at ~170 cm^{-1} appears to be much more sensitive to strain. The following empirical relationship between the RBM frequency, ε_{RBM}, and the diameter of SWNT, d_t, has previously been derived: $\varepsilon_{RBM} = A/d_t + B$.[21,22] Using this relationship and the typical values of A = 234 cm^{-1}, B = 10 cm^{-1}, the diameter of SWNTs in these experiments is estimated to be in the range of 1.3−1.8 nm. These values have a strong correlation to the AFM measurements reported in our previous work.[23]

Furthermore, concurrent to the deformation of the SWNT, a Voc across the sample is measured by a Keithley 4200-SCS semiconductor characterization system. To illustrate this phenomenon, an experiment represented by the plot showing the evolution of this voltage over time is performed (Figure 3). Here, the separation distance, H, is controlled at values of 1.2, 0.6, and 0.3 mm, shown in navy, blue, and red, respectively. For simplicity, this plot can be divided into three time segments. A droplet is placed on the film in the first segment, and the Voc changed from 0 to approximately −200 μV, forming a capillary bridge. A sharp increase in the Voc is observed in the second segment, in which the capillary bridge shrinks toward the center of the film. In the third segment, SWNT films are restored to their free-standing state and the value of Voc is close to zero. During this deformation, several $I-V$ curves are obtained that marked a 19% change in the SWNT film resistance between the free-standing (~199 Ω) and the maximum strain (~236 Ω) states (see Figure S5, Supporting Information). Different droplets, such as methanol and acetone, can also drag the SWNT film down and generate similar mechanical and electrical responses. The measurements can be well repeated (see Figure S6, Supporting Information).

To evaluate the origin of the Voc, the response of the device under different current biases is examined. In these experiments, ethanol droplets are used and a constant separation distance of 12 mm is set for each experiment. Six different current biases, in the range of −20 to 20 μA, are applied to the devices (Figure 4a−f). The red arrows indicate the time at which the maximum strain and its corresponding voltage in the SWNT film have been reached. The voltage increases back to its initial value when the ethanol is completely evaporated from the substrate. As presented in Figure 4g, the device generates a voltage of roughly 500−600 μV at its maximum strain level for the varying current biases. If the Voc relates to the value of resistance, there would be a significant variation in the voltage. This result confirms that

dx.doi.org/10.1021/nl201910j |Nano Lett. 2011, 11, 5117–5122

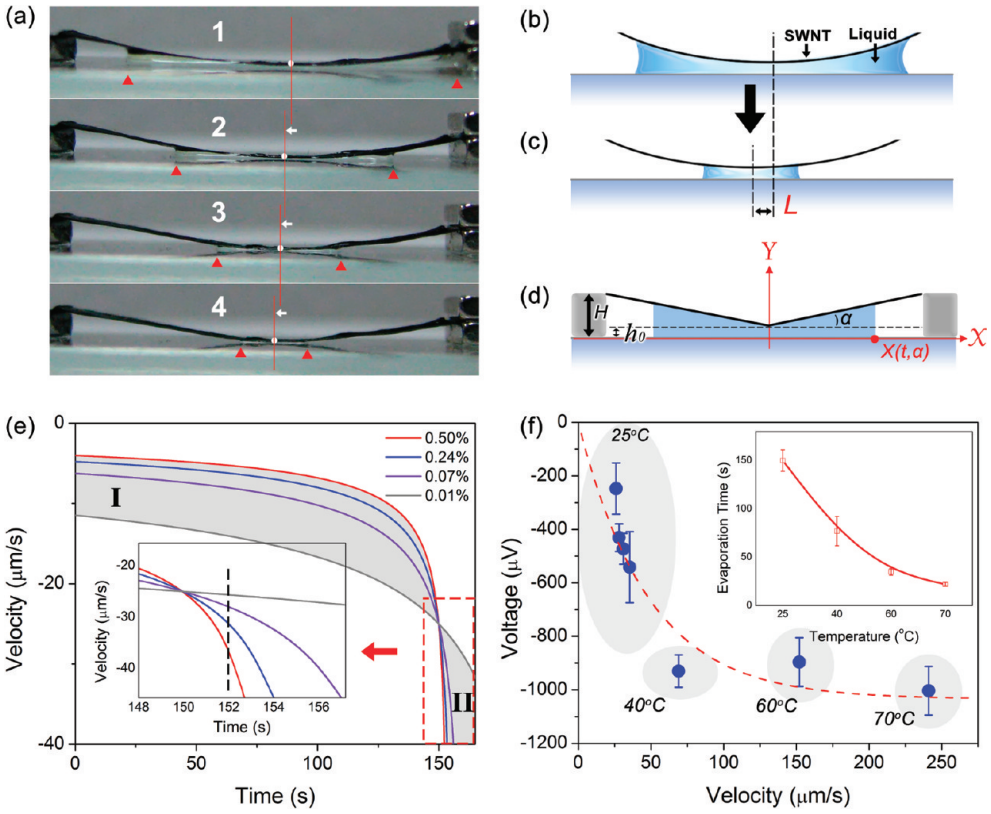

Figure 5. Correlation between the voltage and the induced strain. (a) Consecutively captured photos 1−4 showing the relative movement of midpoints of capillary bridges. Triangles and solid line in red mark both ends and the midpoints of them. White arrows indicate that the midpoints of capillary bridges move to the left during evaporation. (b, c) A displacement of L of the midpoint of capillary bridges. (d) Illustration of the capillary bridge model. (e) Plot of the velocity (midpoint of capillary bridges) versus time based on the model in d, showing distinctive behaviors in time regions I and II. Solid lines in red, blue, purple, and gray correspond to strains of 0.50%, 0.24%, 0.07%, and 0.01%. (f) Plot of induced voltage versus velocity (midpoint of capillary bridges). The data are obtained from 25 to 70 °C as marked by the gray areas. Dash line in red is fitted based on fluctuating Coulombic field. Inset shows the evaporation time of droplets at different temperatures.

the changes in voltage are caused by an electromotive force (EMF, the Voc) and are potentially correlated to the strain in the SWNT films. To rule out the thermoelectric effect on the Voc, the temperature difference of the electrodes at the two ends of the SWNT films is measured, which reflects on a minute value and excludes the possibility of the Voc generated from the thermoelectric effect (see Figure S7, Supporting Information).

It is important to figure out how the Voc correlates with the induced strain. We noticed that there was relative movement of capillary bridge along the SWNT films during the evaporation. The midpoint of the capillary bridge shifted a noticeable distance during evaporation, as demonstrated in Figure 5a, from 1 to 4. This shift originates from the relative misalignment of the two electrodes and could be controlled by adjusting the height difference between the two ends of the film (see Figure S8, Supporting Information). The red triangles mark both ends of the liquid and the red lines specify the midpoint of the film, while arrows displayed how the capillary bridge moved following time. Such movement is illustrated by panels b and c of Figure 5. Figure 5d represents a model for this configuration including SWNT films, substrate, and capillary bridge, which is used to determine the time and strain dependency of the capillary bridge's midpoint velocity. To simplify this problem, it is reasonable to assume that the displacement of the midpoint, $L(t, \alpha)$, is proportional to the location of the capillary bridge, $x(t, \alpha)$. Therefore, we have

$$u(t,\alpha) = \frac{dL}{dt} = \frac{L_0}{X_0} v(t,\alpha) \quad (2)$$

where $u(t, \alpha)$ or $v(t, \alpha)$ is the velocity and $L(t, \alpha)$ or $x(t, \alpha)$ is the displacement of the midpoint, measured from the right-hand side of the capillary bridge. L_0 (~1 mm) is the total displacement of the capillary bridge's middle point, and X_0 (~10 mm) is the initial displacement from the right-hand side of the capillary bridge. The cross-sectional area enclosed between the substrate and the lowest point of a SWNT film consists of two segments: a rectangular area and two trapezoidal areas on top. With these definitions, the following relationship is derived to determine the changing volume of the capillary bridge

$$V_0 - \rho t = \left[\frac{1}{2} x(t,\alpha)^2 \tan(\alpha) W + x(t,\alpha) h_0 W\right] \times 2 \quad (3)$$

where V_0 is the volume of the capillary bridges (~30 μL), ρ represents the evaporation rate of the capillary bridge (V_0/t ~ 0.2 μL/s), h_0 is the height of the rectangular segment (the distance between the substrate and the lowest point of the film, assuming to be 0.2 mm), α is the slant angle between the SWNT film and the substrate (6.8°, 4.6°, 2.9°, and 1.1°), W represents the width of the film (2 mm), and x_0 is the initial distance from the right-hand side of the capillary bridge. The velocity of the

dx.doi.org/10.1021/nl201910j |Nano Lett. 2011, 11, 5117–5122

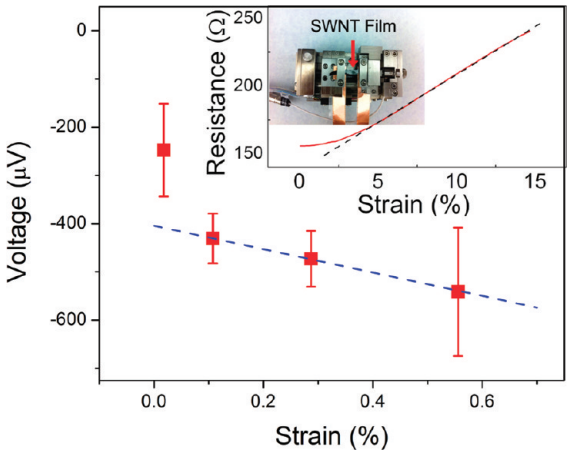

Figure 6. Plot of voltage versus strain. Dash line in blue is a linear fitting within a strain range from 0.1% to 0.6%. Inset shows a SWNT film loaded in a microtester and the plot of resistance versus strain.

midpoint of the capillary bridge is calculated to be (see Figure S9, Supporting Information)

$$u(t,\alpha) = -\frac{L_0}{x_0(\alpha)} \frac{2\rho}{W\sqrt{h_0^2 + 4(x_0(\alpha)^2 \tan(\alpha) + x_0(\alpha)h_0) - \frac{\rho}{W}\tan(\alpha)t}} \quad (4)$$

Considering $V_0 = 2x_0(\alpha)h_0\, W + x_0(\alpha)^2 \tan(\alpha)W$, we have

$$x_0(\alpha) = \left[-h_0 + \sqrt{h_0^2 + \tan(\alpha)\frac{V}{W}}\right]/\tan(\alpha) \quad (5)$$

The plot of time and strain dependence of the capillary bridge's midpoint velocity is shown in Figure 5e. Larger strains result in lower initial velocities, and as the liquid evaporates, the velocity rapidly increases (area I). These changes are more rapid in higher strained samples (area II). The inset provides a close-up of the designated area of the graph in Figure 5e. Such behavior is in good agreement with the plot shown in Figure 3 if associating the velocity with induced voltage. It has been shown that free charge carriers in the nanotubes are dragged by the fluctuating Columbic field of flowing liquid.[24] The motion of the midpoint is a result of a net unidirectional liquid flow. Therefore, we anticipate observing an induced voltage across the film with characteristics reflecting the dynamics of the midpoint's position. The generated voltage can be estimated using the relationship[24]

$$U \approx U_0(1 - e^{-au})/e^{-bu} \quad (6)$$

where u is the velocity of the midpoint of the capillary, derived from eq 4, and U_0, a, and b are fitting parameters. As shown in Figure 5f, this relationship is evaluated by a series of experiments at different temperatures. Voc values are acquired at room temperature (25 °C) for H values 12, 9, 6, and 3 mm, and at temperatures of 40, 60, and 70 °C for a single H value of 12 mm. Velocities at room temperature were estimated from Figure 5e (152 s, denoted with a dashed line). Velocities at other temperatures are estimated, assuming they are proportional to the total evaporation time of the droplets (inset in Figure 5f). These results correlated well with the previous report,[19] with calculated fitting parameters $U_0 = -1033\ \mu$V, $a = 2 \times 10^4$ s/m, and $b = 5$ s/m.

The unique configuration of such a device allows for definition of a new gauge factor based on voltage instead of resistance: $\beta_{GF}(V) = (\delta V/V_0)/\delta\varepsilon$. The voltage-based gauge factor can be up to ~242 for strains in the range of 0.1−0.6%, as shown in Figure 6. It is comparable to the classic gauge factor (resistance-based) obtained from very thin SWNTs (200−1000)[25,26] and much higher than macroscale SWNT films and commercial metallic foils strain gauges (2−30). For further analysis, the classical gauge factor (resistance-based) of our SWNT films is calculated (Inset of Figure 6). The tensile tests are performed using a microtester (Deben UK, Ltd.). The maximum force and displacement capacities of the microtester are 200 N and 10 mm, with resolutions of 0.01 N and 0.001 mm, respectively. The SWNT film was sealed in plastic films, using copper tapes as electrodes; it is then cut and mounted onto the tensile testing device. The uniaxial tensile tests are conducted under displacement control, and the displacement rate is set at ~0.5 mm/min, corresponding to a strain rate of ~7.2×10^{-4}/s. During the tensile test, the electrical resistance of the samples is measured using a two-point probe method with a Keithley 2400 source meter. The initial resistance of the free SWNT film is ~156 Ω. It increases during the tensile test and reaches ~240 Ω, under a tensile strain of ~15%. The gauge factor can be estimated as ~7.1, comparable to pristine macroscale SWNT[27] and ZnO.[28]

In conclusion, we have demonstrated the use of droplets to actuate strain in SWNT films with values ranging from ~0.6% to less than 0.1%. The strain is caused by a wetting force from liquid capillary bridge between suspended SWNT films and substrates. The strain was further confirmed by dynamic Raman spectroscopy and analyzed by the two-dimensional correlation spectra. We reported on a simultaneous dynamic voltage across the SWNT films that emerged during droplet evaporation. Our calculations demonstrated the evolution of the liquid capillary bridge over time and varied strain. Further, these calculations correlate the observed strain to the open-circuit voltage in the physical context of fluctuating Columbic fields. Additionally, as a consequence of the design advantages of our system, a new gauge factor with respect to the changes in voltage was defined, which could lead to a potential high-performance strain sensor of SWNTs.

■ ASSOCIATED CONTENT

Ⓢ Supporting Information. Preparation of SWNT film and fabrication of suspended SWNT film devices, estimation of the strain and tensile force in the SWNT films, I-V characteristics of SWNT film during its deformation, repeated experiments of Voc vs time, temperature difference between both electrodes after dropping liquid on SWNTs, Voc induced by adjusting the height difference between the two ends of the SWNT film, and determination of the velocity of the midpoint of capillary bridges along the SWNT films. This material is available free of charge via the Internet at http://pubs.acs.org.

■ AUTHOR INFORMATION

Corresponding Author

*E-mail: zheng.liu@rice.edu (Zheng Liu), slf@nanoctr.cn (Lianfeng Sun), jlou@rice.edu (Jun Lou); ajayan@rice.edu (Pulickel M. Ajayan).

■ ACKNOWLEDGMENT

L.F.S. acknowledges support from the National Science Foundation of China (Grant No. 10774032, 9092100, 11174062). P.M.A.

acknowledges support from Rice University startup funds and funding support from the Office of Naval Research (ONR) through the MURI program on graphene and the Basic Energy Sciences division of the Department of Energy (DOE). J.L. acknowledges the support of Welch Foundation Grant C-1716, the NSF grants CMMI-0800896 and CMMI-0928297, and the Air Force Research Laboratory Grant AFRL FA8650-07-2-5061. Z.L. was supported by DOEBES program DE-SC0001479 for growth and characterization.

REFERENCES

(1) Zhang, M.; Fang, S.; Zakhidov, A. A.; Lee, S. B.; Aliev, A. E.; Williams, C. D.; Atkinson, K. R.; Baughman, R. H. Strong, Transparent, Multifunctional, Carbon Nanotube Sheets. *Science* **2005**, *309* (5738), 1215–1219.

(2) Li, Z. L.; Dharap, P.; Nagarajaiah, S.; Barrera, E. V.; Kim, J. D. Carbon nanotube film sensors. *Adv. Mater.* **2004**, *16* (7), 640.

(3) Sreekumar, T. V.; Liu, T.; Kumar, S.; Ericson, L. M.; Hauge, R. H.; Smalley, R. E. Single-wall carbon nanotube films. *Chem. Mater.* **2003**, *15* (1), 175–178.

(4) Yamada, T.; Hayamizu, Y.; Yamamoto, Y.; Yomogida, Y.; Izadi-Najafabadi, A.; Futaba, D. N.; Hata, K. A stretchable carbon nanotube strain sensor for human-motion detection. *Nat. Nanotechnol.* **2011**, *6* (5), 296–301.

(5) Chang, N. K.; Su, C. C.; Chang, S. H. Fabrication of single-walled carbon nanotube flexible strain sensors with high sensitivity. *Appl. Phys. Lett.* **2008**, *92*, 063501.

(6) Paulson, S.; Falvo, M. R.; Snider, N.; Helser, A.; Hudson, T.; Seeger, A.; Taylor, R. M.; Superfine, R.; Washburn, S. In situ resistance measurements of strained carbon nanotubes. *Appl. Phys. Lett.* **1999**, *75* (19), 2936–2938.

(7) Dharap, P.; Li, Z.; Nagarajaiah, S.; Barrera, E. V. Nanotube film based on single-wall carbon nanotubes for strain sensing. *Nanotechnology* **2004**, *15* (3), 379–382.

(8) Zhang, X.; Liu, T.; Sreekumar, T. V.; Kumar, S.; Moore, V. C.; Hauge, R. H.; Smalley, R. E. Poly(vinyl alcohol)/SWNT Composite Film. *Nano Lett.* **2003**, *3* (9), 1285–1288.

(9) Salvetat, J. P.; Briggs, G. A. D.; Bonard, J. M.; Bacsa, R. R.; Kulik, A. J.; Stockli, T.; Burnham, N. A.; Forro, L. Elastic and shear moduli of single-walled carbon nanotube ropes. *Phys. Rev. Lett.* **1999**, *82* (5), 944–947.

(10) Walters, D. A.; Ericson, L. M.; Casavant, M. J.; Liu, J.; Colbert, D. T.; Smith, K. A.; Smalley, R. E. Elastic strain of freely suspended single-wall carbon nanotube ropes. *Appl. Phys. Lett.* **1999**, *74* (25), 3803–3805.

(11) Ma, W. J.; Song, L.; Yang, R.; Zhang, T. H.; Zhao, Y. C.; Sun, L. F.; Ren, Y.; Liu, D. F.; Liu, L. F.; Shen, J.; Zhang, Z. X.; Xiang, Y. J.; Zhou, W. Y.; Xie, S. S. Directly Synthesized Strong, Highly Conducting, Transparent Single-Walled Carbon Nanotube Films. *Nano Lett.* **2007**, *7* (8), 2307–2311.

(12) Gruner, G. Carbon nanotube films for transparent and plastic electronics. *J. Mater. Chem.* **2006**, *16* (35), 3533–3539.

(13) Wei, J.; Zhu, H.; Li, Y.; Chen, B.; Jia, Y.; Wang, K.; Wang, Z.; Liu, W.; Luo, J.; Zheng, M.; Wu, D.; Zhu, Y.; Wei, B. Ultrathin Single-Layered Membranes from Double-Walled Carbon Nanotubes. *Adv. Mater.* **2006**, *18* (13), 1695–1700.

(14) Vagharchakian, L.; Restagno, F.; Lger, L. Capillary Bridge Formation and Breakage: A Test to Characterize Antiadhesive Surfaces. *J. Phys. Chem. B* **2008**, *113* (12), 3769–3775.

(15) Yang, W.; Wang, R.-Z.; Yan, H. Strain-induced Raman-mode shift in single-wall carbon nanotubes: Calculation of force constants from molecular-dynamics simulations. *Phys. Rev. B* **2008**, *77* (19), 195440.

(16) Lee, S. W.; Jeong, G.-H.; Campbell, E. E. B. In situ Raman Measurements of Suspended Individual Single-Walled Carbon Nanotubes under Strain. *Nano Lett.* **2007**, *7* (9), 2590–2595.

(17) Dresselhaus, M. S.; Jorio, A.; Hofmann, M.; Dresselhaus, G.; Saito, R. Perspectives on Carbon Nanotubes and Graphene Raman Spectroscopy. *Nano Lett.* **2010**, *10* (3), 751–758.

(18) Cronin, S. B.; Swan, A. K.; Ünlü, M. S.; Goldberg, B. B.; Dresselhaus, M. S.; Tinkham, M. Resonant Raman spectroscopy of individual metallic and semiconducting single-wall carbon nanotubes under uniaxial strain. *Phys. Rev. B* **2005**, *72* (3), 035425.

(19) Ajayan, P. M.; Schadler, L. S.; Giannaris, C.; Rubio, A. Single-Walled Carbon Nanotube−Polymer Composites: Strength and Weakness. *Adv. Mater.* **2000**, *12* (10), 750–753.

(20) Noda, I.; Ozaki, Y. *Two-Dimensional Correlation Spectroscopy: Applications in Vibrational and Optical Spectroscopy*; John Wiley & Sons: Hoboken, NJ, 2004.

(21) Milnera, M.; Kürti, J.; Hulman, M.; Kuzmany, H. Periodic Resonance Excitation and Intertube Interaction from Quasicontinuous Distributed Helicities in Single-Wall Carbon Nanotubes. *Phys. Rev. Lett.* **2000**, *84* (6), 1324.

(22) Kuzmany, H.; Plank, W.; Hulman, M.; Kramberger, C.; Grüneis, A.; Pichler, T.; Peterlik, H.; Kataura, H.; Achiba, Y. Determination of SWCNT diameters from the Raman response of the radial breathing mode. *Eur. Phys. J. B* **2001**, *22* (3), 307–320.

(23) Zhao, Y. C.; Song, L.; Deng, K.; Liu, Z.; Zhang, Z. X.; Yang, Y. L.; Wang, C.; Yang, H. F.; Jin, A. Z.; Luo, Q.; Gu, C. Z.; Xie, S. S.; Sun, L. F. Individual Water-Filled Single-Walled Carbon Nanotubes as Hydroelectric Power Converters. *Adv. Mater.* **2008**, *20* (9), 1772–1776.

(24) Ghosh, S.; Sood, A. K.; Kumar, N. Carbon Nanotube Flow Sensors. *Science* **2003**, *299* (5609), 1042–1044.

(25) Cao, J.; Wang, Q.; Dai, H. Electromechanical Properties of Metallic, Quasimetallic, and Semiconducting Carbon Nanotubes under Stretching. *Phys. Rev. Lett.* **2003**, *90* (15), 157601.

(26) Stampfer, C.; Helbling, T.; Obergfell, D.; Schöberle, B.; Tripp, M. K.; Jungen, A.; Roth, S.; Bright, V. M.; Hierold, C. Fabrication of Single-Walled Carbon-Nanotube-Based Pressure Sensors. *Nano Lett.* **2006**, *6* (2), 233–237.

(27) Haibo, Z.; et al. Carbon nanotube yarn strain sensors. *Nanotechnology* **2010**, *21* (30), 305502.

(28) Gullapalli, H.; Vemuru, V. S. M.; Kumar, A.; Botello-Mendez, A.; Vajtai, R.; Terrones, M.; Nagarajaiah, S.; Ajayan, P. M. Flexible Piezoelectric ZnO−Paper Nanocomposite Strain Sensor. *Small* **2010**, *6* (15), 1641–1646.